ISSN 1392-1207. MECHANIKA. Vol. 32, No. 2, 2026: 140–151

Study on the Rehabilitation Performance of 2-SPS-RRR Adjustable Hip Exoskeleton

Yaohong ZHAO*, Yunfan ZHANG, Yao GAO***, Ruiqin LI*****

**School of Innovation and Entrepreneurship, North University of China, Taiyuan, China,030051, E-mail: zyh-zyh@nuc.edu.cn (Corresponding Author)*

***School of Mechanical Engineering, North University of China, Taiyuan, China,030051, E-mail: 2228584056@qq.com*

****School of Mechanical Engineering, North University of China, Taiyuan, China,030051*

https://doi.org/10.5755/j02.mech.44095

1. Introduction

With the progress of science and technology and the improvement of the environment, the global per capita life expectancy has generally increased, and the aging of the population has become increasingly significant [1]. Low back pain caused by aging is the main cause of disability, which makes the daily life of many elderly people unbearable [2]. Low back pain is closely related to the activity of the human hip joint [3], and the damage of the hip joint has become a major obstacle to the cure of low back pain. Rehabilitation medicine research has found that intensive exercises through repetitive movements can help improve joint strength and promote joint function recovery. At present, rehabilitation doctors are in short supply and expensive to hire. Compared with human rehabilitation, hip joint rehabilitation robots have a new way of rehabilitation for people with hip joint injury due to their high efficiency, specialization and human-robot interaction [4].

At present, series hip exoskeleton is still the main force in this field. Yu et al. [5] developed a collimated-drive hip exoskeleton. Zhou et al. [6] designed an unpowered hip exoskeleton. Kawashima et al. [7] designed a Honda stride management assist device. The Institute of Automation, Chinese Academy of Sciences (CAS) et al. [8-10] developed an APO exoskeleton.

However, compared with the series mechanism, the parallel mechanism has become the best choice for the hip rehabilitation exoskeleton structure with its advantages of good stability, high stiffness and high motion accuracy. Wang et al. [11, 12] designed a biological fusion hip exoskeleton based on 2-UPS+S (Numbers represent the number of branches, U represents a Hooke joint, P represents a prismatic joint, and S represents a spherical joint. The same applies below) parallel mechanism. The exoskeleton equates the human hip joint as a spherical joint and forms a complete parallel mechanism with 2-UPS parallel mechanism to assist the human body. Xu et al. [13] designed a biological fusion type of medullary joint exoskeleton based on 3-RRPS/S (R represents a revolute joint, and the same applies below) parallel mechanism, which also equivalent the hip joint to a spherical joint and works together with 3-RRPS parallel mechanism, reducing the nonlinear degree of the exoskeleton input and output, making the exoskeleton have certain motion decoupling characteristics, which is conducive to motion control and improving the force transmission performance of the exoskeleton. Shi D et al. [14] proposed a 2-UPS/RRR parallel hip rehabilitation mechanism with virtual transmission center, which can realize three degrees of freedom motion of human hip joint sagittal plane movements, frontal plane movements and transverse plane movements. Li et al. [15] designed a two-degree-of-freedom parallel hip joint assist mechanism with two UPS+UPR branched chains to assist the human hip joint in sagittal plane movements and frontal plane movements. Jia et al. [16] proposed a rehabilitation parallel mechanism with two degrees of freedom to realize the decoupling motion of flexion extension and retraction at the hip joint, reducing the control difficulty. Huang et al. [17] designed a 4-UPUR+RR parallel structure of hip rehabilitation exoskeleton, which realized the decoupling of hip rotation and movement, and improved the human-robot interaction performance of the exoskeleton.

The above-mentioned hip exoskeleton can be roughly divided into two types: biological fusion type and bionic type. The former takes the human hip joint as a spherical joint to participate in the assist process of the exoskeleton, so that the motion of the hip joint can be determined. Without the participation of the hip joint, the mechanism has six degrees of freedom. The latter simulates the three rotational degrees of freedom of the human hip joint to design a parallel hip exoskeleton with two or three degrees of freedom, allowing the mechanism to have two or three directions of assistance. However, the biological fusion exoskeleton of the hip joint forces the human hip joint to participate in the movement of the whole mechanism, so that the human hip joint has to bear a certain force, which has a certain use pressure for the people whose hip joints have been damaged, but it does have a good help effect for the people with healthy hip joints, and always keeps the motion center of the mechanism coincide with the rotation center of the human hip joint, which indicates that this kind of exoskeleton is more suitable for the help of healthy people or the extreme movement beyond the force range borne by people. Although the bionic exoskeleton does not have the characteristics of keeping the motion center of the mechanism and the rotation center of the human hip joint always coincide, it can avoid the human hip joint from bearing large pressure and fully meet the rotation requirements of the human hip joint in a small range, such as the 3-RRR spherical parallel mechanism, which has the advantages of miniaturization and lightweight in addition to the advantages of parallel mechanism [18,19], which has more prominent advantages in the field of hip rehabilitation, can reduce the user's burden and promote the rehabilitation training; The driving of the revolute pair of the 3-RRR mechanism is a revolute pair, and its bearing capacity is slightly insufficient. The parallel mechanism configuration with direct connection between the

moving platform and the static platform has the characteristics of high stiffness and strong bearing capacity [20]. Therefore, 2-SPS-RRR mechanism with the advantages of spherical mechanism and mobile driving is more suitable for the application of hip rehabilitation exoskeleton.

In this paper, a wearable spherical parallel hip exoskeleton with adjustable rotation center is designed based on 2-SPS-RRR parallel mechanism. The exoskeleton has the advantages of large rotation space, high dexterity, adjustable rotation center, strong bearing capacity, simple structure and easy control in the rehabilitation training of human hip joint. The mechanism can assist the human hip joint in sagittal plane movements, frontal plane movements and transverse plane movements, and improve the rehabilitation efficiency of the user's damaged hip joint.

2. Human Hip Joint Motion Under Normal Walking Based on AnyBody

The hip joint is the largest and most weight-bearing joint in the human body [21]. As a multi axial joint, it can achieve sagittal plane movements, frontal plane movements and transverse plane movements, as shown in Fig. 1. During walking, the sagittal plane movements of the hip joint can help the body move forward in a straight line, the frontal plane movements of the hip joint can coordinate the body's position and the transverse plane movements of the hip joint can assist the body in turning.

The ergonomics and biomechanical analysis software AnyBody has powerful functions in analyzing the characteristics of the human skeletal muscle system and tendons [22]. In this paper, the motion mode of the human body under normal walking was loaded into AnyBody software and the motion curve of the hip joint was obtained as shown in Fig. 2. From the curves, it can be seen that during normal walking, the hip joint undergoes sagittal plane movements around the coronal axis with a rotation angle between -30° and 18°; The rotation angle of the frontal plane movements around the sagittal axis is between -10° and 10°; The transverse plane movements around the vertical axis has a relatively smaller range of rotation angles compared to the previous two, with rotation angles ranging from –5° to 6°.

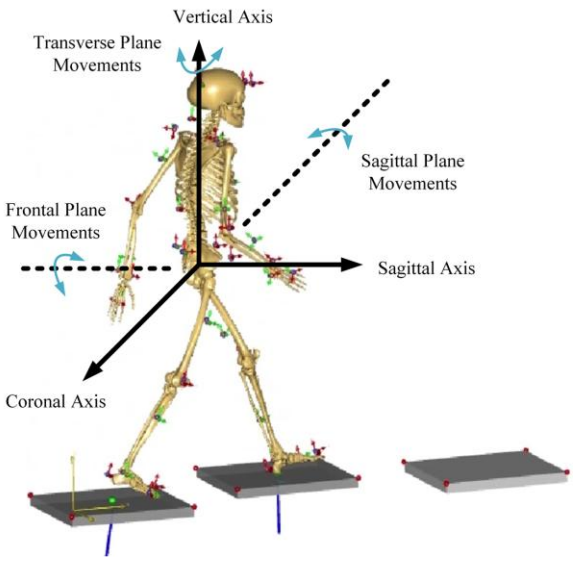

Fig. 1 Hip joint motion pattern

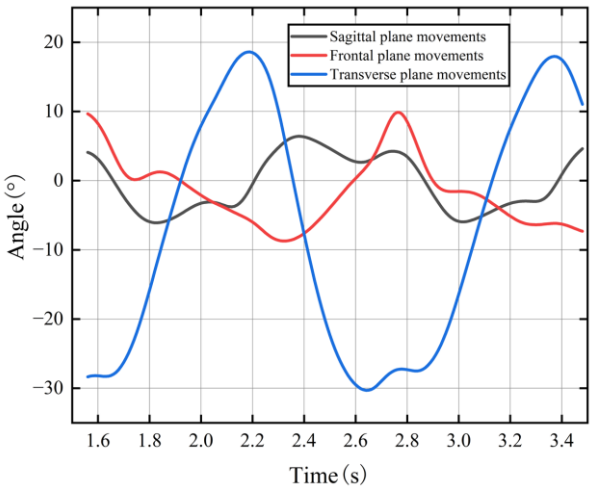

Fig. 2 Range of hip joint movement angle

3. Structure Design of Adjustable Hip Exoskeleton

Fig. 3 shows the overall model of the exoskeleton of the spherical hip joint. The mechanism is composed of three parts from top to bottom: first, the fixed static platform that directly contacts the waist of the human body and is also the part of the exoskeleton centering mechanism; Secondly, the 2-SPS-RRR parallel mechanism, which is the core part of exoskeleton participating in motion, is the most critical part of exoskeleton undertaking a series of motion tasks. The rotation center of human hip joint and the motion center of mechanism are adjusted and overlapped after wearing; Finally, a fixed moving platform bound to the human thigh. Details are described below.

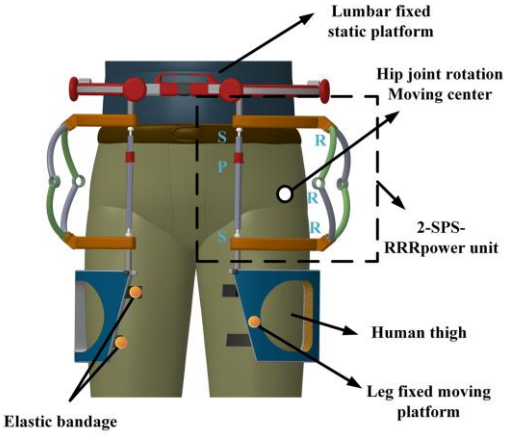

Fig. 3 A holistic model of the rehabilitation mechanism

3.1. Design of adjusting structure of mechanism rotation center

After some hip rehabilitation exoskeletons are worn on the human body, they need to be worn again because the rotation center of the exoskeletons is inconsistent with the rotation center of the human hip. Although some hip exoskeletons can adjust the rotation center, the adjustment structure needs to be manually adjusted by external manpower, which affects the user's rehabilitation experience to a certain extent.

Based on the above situation, this paper designs the rotation center adjustment structure as shown in Fig. 4. The inner part of the ring structure is embedded with a mobile

drive that can move forward and backward, left and right, and up and down. The outer part carries a corresponding drive motor, which can be driven and controlled by a single chip microcomputer. Among them, the driving pair that adjusts the up and down movement is connected with the ring-shaped fixed static platform and 2-SPS-RRR parallel mechanism. One side of the driving pair that adjusts the front and rear left and right movement is embedded in the ring-shaped fixed static platform, and the other side is embedded in the elastic bandage platform that is worn in direct contact with the human body in the form of a guide rail. Before the user puts on the exoskeleton and starts the rehabilitation training, when adjusting the rotation center, the user can control the drive motor connected to the ring-shaped fixed static platform to drive the self-aligning moving pair. The four moving pairs for fore-and-aft direction adjustment, the two moving pairs for left-right direction adjustment and the four moving pairs for up-down direction adjustment run together, and finally realize the self-aligning purpose. After the adjustment is completed, the motor can be locked to lock the self-aligning structure. The fixed static platform is fixedly connected with the static platform of the 2-SPS-RRR parallel mechanism as a whole.

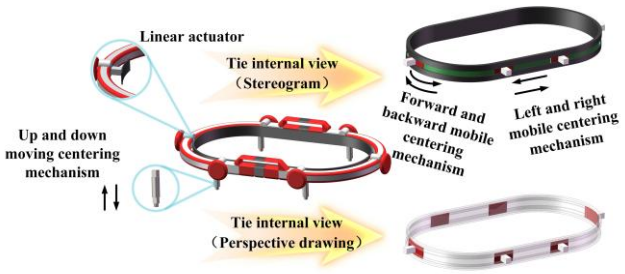

Fig. 4 Mechanism rotation center adjustment structure

3.2. Design of 2-SPS-RRR parallel mechanism

As shown in Fig. 5, the wearable spherical exoskeleton 2-SPS-RRR parallel mechanism is composed of a static platform $A_1A_2A_3$, a moving platform $B_1B_2B_3$, two identical SPS branched chains (branched chain I and branched chain II) and four spherical rods with the same curvature (member I, member II, member III and member IV). The branched chain I is connected to the static platform through the spherical pair S at A_1, and also connected to the moving platform through the spherical pair S at B_1. The upper and lower members of the branched chain I are connected through the prismatic pair P. The connection mode of the branched chain II is exactly the same as that of the branched chain I.

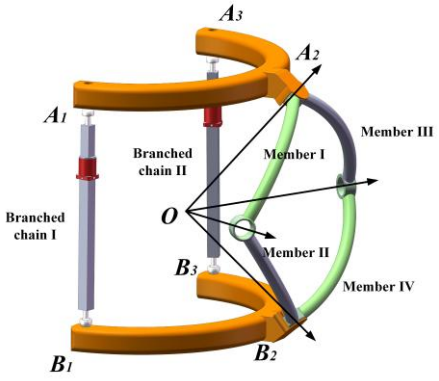

Fig. 5 2-SPS-RRR parallel mechanism

The members I and III are connected to the static platform through the revolute pair R at A_2, the members II and IV are also connected to the moving platform through the revolute pair R at B_2, the members I and II are connected through the revolute pair R, and the members III and IV are connected through the revolute pair R. The curvature center of the members I, II, III and IV is point O. Because bar III and bar IV play exactly the same role as member I and member II in addition to improving the stability of the mechanism during operation, the mechanism is essentially a 2-SPS-RRR spherical hip joint parallel mechanism.

3.3. Design of fixed moving platform bound to legs

The fixed moving platform and 2-SPS-RRR parallel mechanism are also connected by the driving pair that adjusts the up and down movement. This part can carry out the up and down, front and back, left and right follow-up movement when the fixed static platform is aligned. After the fixed static platform is aligned, the user can drive the motor to lock the follow-up pair. The fixed moving platform is fixedly connected with the moving platform of 2-SPS-RRR parallel mechanism as a whole.

4. Kinematics of the Spherical Hip Joint

4.1. The degree of freedom of the mechanism

First, the corresponding coordinate system is established on the mechanism shown in Fig. 6: the spatial rectangular coordinate system is established with the spherical center O of the spherical hip joint parallel mechanism as the origin, OZ axis is vertical upward, OX axis is horizontal to the right, and the establishment of OY axis conforms to the right-hand coordinate system rule; The coordinate system A_1-xyz is established on the branched chain I, in which A_1z axis, A_1x axis and A_1y axis are parallel to OZ axis, OX axis and OY axis and have the same direction.

The degree of freedom of 2-SPS-RRR parallel mechanism is analyzed using screw theory [23, 24]. The kinematic pair is represented by the form of the screw of the kinematic pair, and the degree of freedom of the mechanism is solved by analyzing the screw of these kinematic pairs.

According to screw theory, the kinematic screw system of branched chain I is:

$$\begin{cases} \$_{11} = (1,0,0;0,0,0) \\ \$_{12} = (0,1,0;0,0,0) \\ \$_{13} = (0,0,1;0,0,0) \\ \$_{14} = (0,0,0;0,0,z_1) \\ \$_{15} = (1,0,0;0,z_2,0) \\ \$_{16} = (0,1,0;-z_2,0,0) \\ \$_{17} = (0,0,1;0,0,0) \end{cases} . \tag{1}$$

It can be seen from the moving screw system of branched chain I, $\$_{13}$ and $\$_{17}$ are exactly the same, and it is not linearly correlated with the other five pairs of screw. According to the reciprocity screw theory, the branched chain has no constraint on the position and orientation changes of the moving platform. In the same way, the branched chain II has no constraint on the position and attitude changes of

the moving platform.

The four revolute pairs located in the spherical surface of the mechanism can be expressed as follows according to the screw theory:

$$\begin{cases} \$_{31} = (a_1, 0, c_1; 0, 0, 0) \\ \$_{32} = (a_2, b_2, 0; 0, 0, 0) \\ \$_{33} = (a_3, 0, c_3; 0, 0, 0) \\ \$_{34} = (a_4, b_4, 0; 0, 0, 0) \end{cases}. \tag{2}$$

And the reciprocal product of the moving screw and the constrained screw is zero, thus the three anti screws of Eq. (2) are

$$\begin{cases} \$_{31}^{r} = (1, 0, 0; 0, 0, 0) \\ \$_{32}^{r} = (0, 1, 0; 0, 0, 0) \\ \$_{33}^{r} = (0, 0, 1; 0, 0, 0) \end{cases}. \tag{3}$$

The reverse screw of Eq. (3) can be obtained, and the kinematic screw system of the whole mechanism is:

$$\begin{cases} \$_{31}^{rr} = (1, 0, 0; 0, 0, 0) \\ \$_{32}^{rr} = (0, 1, 0; 0, 0, 0) \\ \$_{33}^{rr} = (0, 0, 1; 0, 0, 0) \end{cases}, \tag{4}$$

To sum up, 2-SPS-RRR spherical hip joint parallel mechanism has three rotational degrees of freedom around x axis, y axis and z axis, and the modified G-K formula shown in Eq. 5 verifies the correctness of the degree of freedom solution.

$$M = d(n - g - 1) + \sum_{i=1}^{g} f_i + \nu - \zeta = 3, \tag{5}$$

where, M is the degree of freedom of the mechanism; the mechanism has no public constraint, the order of the mechanism is $d = 6$; n is the number of components including the rack, $n = 8$; g is the number of motion pairs, $g = 9$; f_i is the number of degrees of freedom of the i_{th} kinematic pair; there is no parallel redundancy constraint in the mechanism, $\nu = 0$. There are two local degrees of freedom in the mechanism, $\zeta = 2$.

4.2. Inverse solution analysis of the mechanism position

The closed vector method is used to analyze the inverse position of 2-SPS-RRR parallel mechanism.

As shown in Fig. 6, a static coordinate system O_1-$X_1Y_1Z_1$ is established at the center of the static platform, where O_1X_1 axis points to A_1, O_1Y_1 axis points to A_2, and O_1Z_1 axis is determined by the right-hand rule. Since the rotation center of the three rotational degrees of freedom of the mechanism is located at the center of the RRR spherical rod, and in order to avoid unnecessary concomitant movement, a dynamic coordinate system O-XYZ is established at the center of the RRR spherical branch, where the OX axis, OY axis, and OZ axis are parallel to the O_1X_1 axis, O_1Y_1 axis, and O_1Z_1 axis, respectively, and the directions are consistent. The circumference radius of the moving platform is R, and the circumference radius of the static platform is r.

Define the rotation angles of moving platform $B_1B_2B_3$ around OX OY and OZ axes are respectively expressed in ψ, θ and ϕ, S_1 and S_2 are the axes of the rotation pairs at A_2 and B_2, S_1 and S_2 axes can be regarded as the rotation equivalent axes of the spherical mechanism, and the rotation angles of the S_1 and S_2 axes are respectively expressed in θ_1 and θ_2. The intersection with S_1 and S_2 is the spherical center O of the RRR spherical branched chain. When the mechanism is in the initial position, the moving platform is parallel to the static platform, the quadrilateral composed of four points $A_1B_1B_3A_3$ is a rectangle and parallel to the moving and static platform, and the spherical rods I and II and spherical rods III and IV are close to the point O passing through the ball center and perpendicular to both sides of the plane of the quadrilateral $A_1B_1B_3A_3$. Let θ_1 and θ_2 angles at the initial position be 0, the vertical distance from the ball center O to the static and moving platforms be l, and the vertical distance to the quadrilateral $A_1B_1B_3A_3$ be m.

Setting the prismatic pairs in the two SPS branched chains of the mechanism and the revolute pair at B_2 where the RRR branched chain is hinged with the static platform as the driving pair, the relationship between the moving drive P_1, P_2 and angle drive θ_1 and the rotating angles ψ, θ and ϕ of the moving platform can be established.

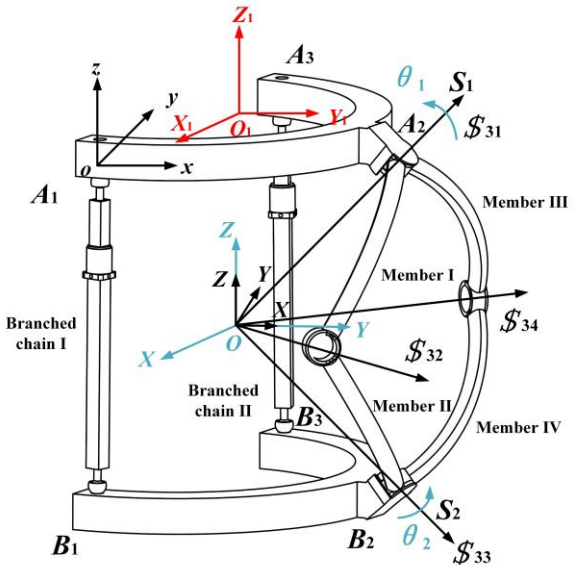

Fig. 6 2-SPS-RRR schematic diagram of inverse coordinate solution for the parallel mechanism

4.2.1. Inverse kinematics solution of 2-SPS

In the static coordinate system O_1-$X_1Y_2Z_3$, the coordinate of the point A_i is

A_1 (R, 0, 0), A_2 (0, R, 0), A_3 (-R, 0, 0)

In the moving coordinate system O-xyz, the coordinate of the point A_i is

B_1 (r, -m, -l), B_2 (0, r-m, -l), B_3 (-r, -m, -l)

The RPY angle is used to represent the rotation transformation matrix R of the moving platform point B_i relative to the static platform point A_i, then the rotation matrix R can be expressed as

$$ {}^{A}_{o}\boldsymbol{R} = \boldsymbol{R}_{XYZ}(\psi,\theta,\phi) = \boldsymbol{Rot}(z,\phi)\,\boldsymbol{Rot}(y,\theta)\,\boldsymbol{Rot}(x,\psi) = \begin{bmatrix} c_\theta c_\phi & s_\psi s_\theta c_\phi - c_\psi s_\phi & c_\psi s_\theta c_\phi + s_\psi s_\phi \\ c_\theta s_\phi & s_\psi s_\theta s_\phi + c_\psi c_\phi & c_\psi s_\theta s_\phi - s_\psi c_\phi \\ -s_\theta & s_\psi c_\theta & c_\psi c_\theta \end{bmatrix}. \quad (6) $$

Here and further in the equations $s_\theta = sin\ \theta$, $s_\phi = sin\ \phi$, $s_\psi = sin\ \psi$, $c_\theta = cos\ \theta$, $c_\phi = cos\ \phi$, $c_\psi = cos\ \psi$.

B_i is represented by B'_i in the static coordinate system, with

$$ \boldsymbol{B}'_i = \begin{bmatrix} \boldsymbol{x}_{B'_i} \\ \boldsymbol{y}_{B'_i} \\ \boldsymbol{z}_{B'_i} \end{bmatrix} = {}^{A}_{o}\boldsymbol{R} \begin{bmatrix} \boldsymbol{x}_{B_i} \\ \boldsymbol{y}_{B_i} \\ \boldsymbol{z}_{B_i} \end{bmatrix} + \boldsymbol{O}. \quad (7) $$

Since the mechanism has no degree of freedom of movement along *X*-axis, *Y*-axis and *Z*-axis during its movement, there is $x = 0$ according to the position relationship between point *O* and point O_1, $y = m$, $z = -l$.

$$ \begin{cases} B'_1 = \begin{pmatrix} rc_\theta c_\phi - m\left(s_\psi s_\theta c_\phi - c_\psi s_\phi\right) - l\left(c_\psi s_\theta c_\phi + s_\psi s_\phi\right) \\ rc_\theta s_\phi - m\left(s_\psi s_\theta s_\phi + c_\psi c_\phi\right) - l\left(c_\psi s_\theta s_\phi - s_\psi c_\phi\right) + m \\ -rs_\theta - ms_\psi c_\theta - lc_\psi c_\theta - l \end{pmatrix}, \\ B'_2 = \begin{pmatrix} (r-m)\left(s_\psi s_\theta c_\phi - c_\psi s_\phi\right) - l\left(c_\psi s_\theta c_\phi + s_\psi s_\phi\right) \\ (r-m)\left(s_\psi s_\theta s_\phi + c_\psi c_\phi\right) - l\left(c_\psi s_\theta s_\phi - s_\psi c_\phi\right) + m \\ (r-m)s_\psi c_\theta - lc_\psi c_\theta - l \end{pmatrix}, \\ B'_3 = \begin{pmatrix} -rc_\theta c_\phi - m\left(s_\psi s_\theta c_\phi - c_\psi s_\phi\right) - l\left(c_\psi s_\theta c_\phi + s_\psi s_\phi\right) \\ rc_\theta s_\phi - m\left(s_\psi s_\theta s_\phi + c_\psi c_\phi\right) - l\left(c_\psi s_\theta s_\phi - s_\psi c_\phi\right) + m \\ -rs_\theta - ms_\psi c_\theta - lc_\psi c_\theta - l \end{pmatrix}. \end{cases} \quad (8) $$

Branched chain 2-SPS existence constraint equation $P_i = |B'_i - A_i|$. Therefore, the inverse equation of P_1 and P_2 of the moving pair drive is:

$$ \begin{cases} P_1 = \left|B'_1 - A_1\right| = \sqrt{M_1 + M_2 + M_3} \\ P_2 = \left|B'_3 - A_3\right| = \sqrt{N_1 + N_2 + N_3} \end{cases}, \quad (9) $$

$$ M_1 = \left(r c_\theta c_\phi - m\left(s_\psi s_\theta c_\phi - c_\psi s_\phi\right) - \right. $$
$$ \left. -l\left(c_\psi s_\theta c_\phi + s_\psi s_\phi\right) - R\right)^2, \quad (10) $$

$$ N_1 = \left(-r c_\theta c_\phi - m\left(s_\psi s_\theta c_\phi - c_\psi s_\phi\right) - \right. $$
$$ \left. -l\left(c_\psi s_\theta c_\phi + s_\psi s_\phi\right) + R\right)^2, \quad (11) $$

$$ M_2 = N_2 = \left(r c_\theta s_\phi - m\left(s_\psi s_\theta s_\phi + c_\psi c_\phi\right) - \right. $$
$$ \left. -l\left(c_\psi s_\theta s_\phi - s_\psi c_\phi\right) + m\right)^2, \quad (12) $$

$$ M_3 = N_3 = \left(-rs_\theta - ms_\psi c_\theta - lc_\psi c_\theta - l\right)^2. \quad (13) $$

4.2.2. Inverse kinematics solution of 2-RRR branched chain

In order to solve the inverse solution of the rotation drive θ_1 at A_2, it is advisable to make the vertical plane P_1 of the S_1 axis and intersect it at A_2 point, and then make an isosceles triangle A_2DE with an obtuse angle of 100° in this plane. The vertex is A_2 point, and the straight line of the bottom edge of the triangle A_2DE is located in the plane P_2 of the spherical RRR mechanism passing through the ball center and parallel to the initial position of the moving platform and the static platform, and the vertical line of the bottom edge of the triangle passing through the ball center *O* and intersecting with the bottom edge at point *C*, as shown in Fig. 7. The swing amplitude of the segment A_2C passing through A_2 in the triangle A_2DE during the rotation of the moving platform is the change angle of θ_1. The coordinate of point *C* is $C = (0, R\text{-}m\text{+}l\ tan50°, 0)$.

C is represented by *C′* in the static coordinate system, with

$$ \boldsymbol{C}' = \begin{bmatrix} \boldsymbol{x}_{C'} \\ \boldsymbol{y}_{C'} \\ \boldsymbol{z}_{C'} \end{bmatrix} = {}^{A}_{o}\boldsymbol{R} \begin{bmatrix} \boldsymbol{x}_{C} \\ \boldsymbol{y}_{C} \\ \boldsymbol{z}_{C} \end{bmatrix} + \boldsymbol{O}, \quad (14) $$

$$ C' = \begin{bmatrix} \left(R - m + l\,tan50°\right)\left(s_\psi s_\theta c_\phi - c_\psi s_\phi\right) \\ \left(R - m + l\,tan50°\right)\left(s_\psi s_\theta s_\phi + c_\psi c_\phi\right) + m \\ \left(R - m + l\,tan50°\right))s_\psi c_\theta - l \end{bmatrix}. \quad (15) $$

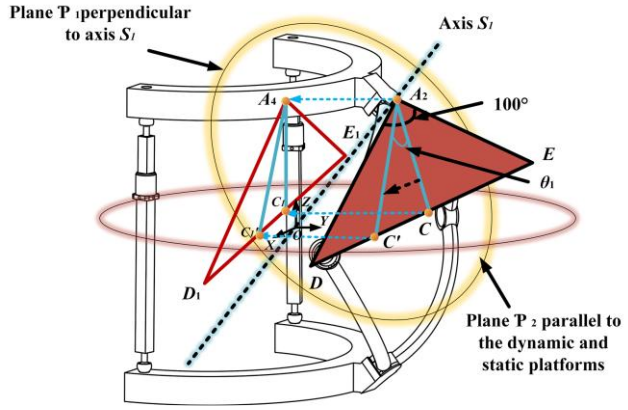

Fig. 7 Schematic diagram of 2-SPS-RRR spherical mechanism

The triangle A_2DE and line segment A_2C are projected to the moving coordinate system O-XYZ as a triangle $A_4D_1E_1$ and line segment A_4C_1. At this time, the swing amplitude of line segment A_2C during the rotation of the moving platform is equivalent to the swing amplitude of line segment A_4C_1 in triangle $A_4D_1E_1$ in the XOZ plane of the moving coordinate system O-XYZ, that is, the angle of change of angle, which can be obtained from the geometric relationship.

$$\begin{aligned} tan\,\theta &= tan\angle C_1'A_4C_1 = \left|C_1C_1'\right| \Big/ \left|C_1A_4\right| = \\ &= \left|x_{C'}\right| \Big/ \left(l_1 - \left|x_{Z'}\right|\right). \end{aligned} \tag{16}$$

Therefore, the inverse equation of θ_1 driven by the revolute pair is:

$$\theta_1 = arctan\angle C_1'A_4C_1 . \tag{17}$$

In this way, the relationship between the movement drive P_1, P_2 and rotation drive θ_1 of the mechanism and the rotation angles ψ, θ and ϕ of the moving platform is established, and the inverse kinematics analysis is completed.

4.3. Velocity Jacobian matrix analysis

By deriving the equations of the inverse solution of the mechanism position from ψ, θ and ϕ respectively, it can be obtained that:

$$\begin{cases} \dfrac{\partial p_1}{\partial \psi} = \dfrac{a_1}{d_1} \\ \dfrac{\partial p_1}{\partial \theta} = \dfrac{b_1}{d_1} \\ \dfrac{\partial p_1}{\partial \phi} = \dfrac{c_1}{d_1} \end{cases} \begin{cases} \dfrac{\partial p_2}{\partial \psi} = \dfrac{a_2}{d_2} \\ \dfrac{\partial p_2}{\partial \theta} = \dfrac{b_2}{d_2} \\ \dfrac{\partial p_2}{\partial \phi} = \dfrac{c_2}{d_2} \end{cases} \begin{cases} \dfrac{\partial \theta_1}{\partial \psi} = \dfrac{a_3}{d_3} \\ \dfrac{\partial \theta_1}{\partial \theta} = \dfrac{b_3}{d_3} \\ \dfrac{\partial \theta_1}{\partial \phi} = \dfrac{c_3}{d_3} \end{cases} . \tag{18}$$

The details of a_1, b_1, c_1, d_1, a_2, b_2, c_2, d_2, a_3, b_3, c_3, d_3 in Eq. (18) are given in the Appendix A at the end of the paper.

The pose parameters ψ, θ and ϕ of the mechanism are functions of time t, so the velocity Jacobian expression is obtained by sorting out the above formula

$$\begin{cases} \dot{P}_1 = \dfrac{a_1\dot{\psi} + b_1\dot{\theta} + c_1\dot{\phi}}{d_1} \\ \dot{P}_2 = \dfrac{a_2\dot{\psi} + b_2\dot{\theta} + c_2\dot{\phi}}{d_2} \\ \dot{\theta}_1 = \dfrac{a_3\dot{\psi} + b_3\dot{\theta} + c_3\dot{\phi}}{d_3} \end{cases} . \tag{19}$$

Rewriting the above formula into matrix form:

$$\boldsymbol{J}_t \begin{bmatrix} \dot{p}_1 \\ \dot{p}_2 \\ \dot{\theta}_1 \end{bmatrix} - \boldsymbol{G} \begin{bmatrix} \dot{\psi} \\ \dot{\theta} \\ \dot{\phi} \end{bmatrix} = 0 , \tag{20}$$

where, matrices $\boldsymbol{J_t}$ and $\boldsymbol{G}$ are respectively:

$$\boldsymbol{J}_t = \begin{bmatrix} d_1 & & \\ & d_2 & \\ & & d_3 \end{bmatrix}, \tag{21}$$

$$\boldsymbol{G} = \begin{bmatrix} a_1 & b_1 & c_1 \\ a_2 & b_2 & c_2 \\ a_3 & b_3 & c_3 \end{bmatrix} . \tag{22}$$

Then the first-order velocity Jacobian matrix of the mechanism is:

$$\boldsymbol{J} = \boldsymbol{J}_t^{-1}\boldsymbol{G} . \tag{23}$$

5. Reachable Workspace Analysis

Workspace is an important indicator to measure the performance of a mechanism. The structural parameters of 2-SPS-RRR hip exoskeleton spherical parallel mechanism are shown in Table 1.

Table 1
Structural parameters of spherical exoskeleton hip joint parallel mechanism

Structure parameters	Numerical value
Circular radius of the static platform	110 mm
Circular radius of the moving platform	110 mm
Distance from the ball center O to the static platform	89 mm
Included angle between axes S_1 and S_2 and the static and the moving platforms	50°
Circular radius of the spherical mechanism	120 mm
Maximum travel of the prismatic pair	115 mm

The rotation angle range of θ_1 and θ_2 is limited to -50° to 50° and the length variation range of the moving auxiliary rod of branched chain I and branched chain II is 130 to 280mm. Set the search range as $-72° \le \psi \le 72°$, $-72° \le \theta \le 72°$, $-72° \le \phi \le 72°$.

Using the numerical search method, the workspace

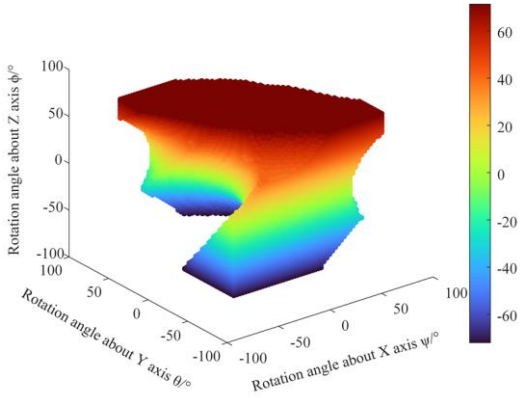

a

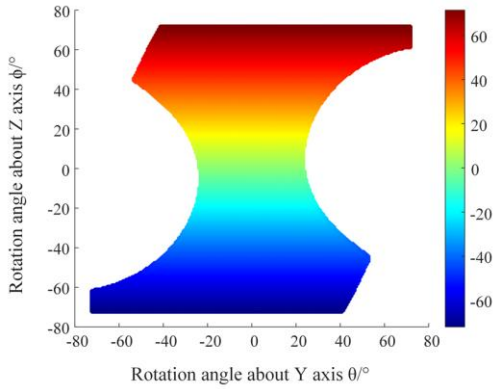

b

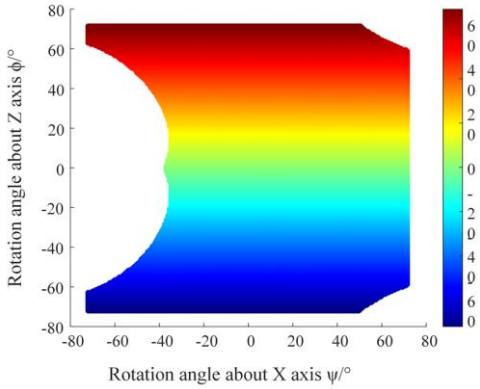

c

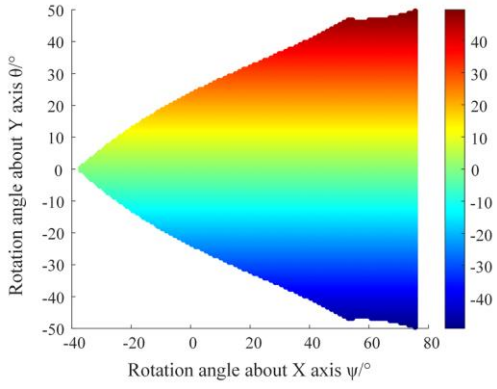

d

Fig. 8 Workspace of the spherical mechanism: a – graphic model, b – cross section when $\psi = 0°$, c – cross section when $\theta = 0°$, d – cross section when $\phi = 0°$

of 2-SPS-RRR parallel mechanism is obtained in MATLAB software, as shown in Fig. 8.

It can be seen from Fig. 8 that the workspace of the mechanism is a polyhedron symmetrical around Z axis, and its interior is continuous without holes. When $\psi = 0°$, the maximum range of sagittal plane movements and transverse plane movements of the moving platform can reach -70°~70°; When $\theta = 0°$, the range of frontal plane movements and transverse plane movements of the moving platform can reach -70°~70°; When $\phi = 0°$, the range of sagittal plane movements and frontal plane movements of the moving platform is -40°~70° and -50°~50°, respectively. Therefore, the mechanism can reach the limit position within the workspace, and the workspace is large, which can meet the needs of human daily movement, and the working performance is good.

6. Performance Analysis of Hip Exoskeleton

6.1. Dexterity analysis

Here, the dexterity of the mechanism is analyzed using the condition number index 25.

The condition number of Jacobian matrix is defined as:

$$\boldsymbol{\kappa}(\boldsymbol{J}) = \boldsymbol{cond}(\boldsymbol{J}) = \frac{\boldsymbol{\sigma}_{\max}(\boldsymbol{J})}{\boldsymbol{\sigma}_{\min}(\boldsymbol{J})}. \tag{24}$$

The value range of the condition number $\boldsymbol{\kappa}(\boldsymbol{J})$ is [1, +∞). Generally, the reciprocal of the condition number of the Jacobian matrix is defined as the local condition number index, that is, the dexterity is

$$\boldsymbol{LCI} = 1/\boldsymbol{cond}(\boldsymbol{\kappa}). \tag{25}$$

Therefore, the value range of $\boldsymbol{LCI}$ is [0, 1]. The dexterity value of the mechanism can be obtained by solving the Jacobian matrix of 3.3 knots. The dexterity maps of the whole region, $\psi = 0°$, $\theta = 0°$ and $\phi = 0°$ can be obtained using MATLAB software, as shown in Fig. 9.

As can be seen from Fig. 9, the range of LCI is [0.1, 0.3]. In the local region, the value of LCI increases with the increase of absolute values of ψ, θ and ϕ; On a global scale, the change of $\boldsymbol{LCI}$ value fluctuates gently without abrupt cusps, indicating that the mechanism has good motion flexibility, can avoid singular configuration, and has good motion performance, which meets the practical application requirements of the rehabilitation parallel mechanism.

6.2. Human-robot coupling simulation based on AnyBody software

The process of AnyBody modeling system mainly carries out biomechanical simulation through two basic methods: mechanical model and muscle model. This study focuses on the application of muscle models.

In order to verify the coupling degree between 2-SPS-RRR parallel mechanism and the human body, and to test the influence of the mechanism on the human muscle, the mechanism model is imported into AnyBody software for simulation, as shown in Fig. 10. The human-robot

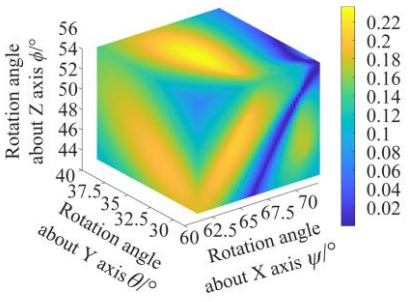

a

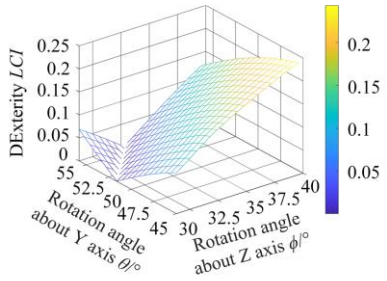

b

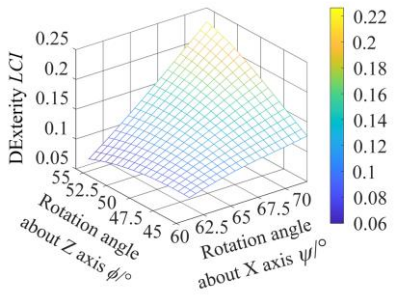

c

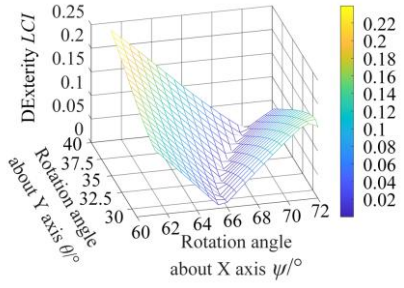

d

Fig. 9 The dexterity atlases: a – global dexterity map, b – dexterity map at $\psi = 0°$, c – dexterity map at $\theta = 0°$, d – dexterity map at $\phi = 0°$

simulation system in AnyBody software can simulate the physiological parameters of the muscle groups that patients mainly participate in during rehabilitation training. Here, the muscle activation parameter is taken to determine whether muscle damage will be caused, and the muscle length change and muscle force change are taken to evaluate the rehabilitation effect. Among them, the most significant change in muscle parameters during human exercise is muscle activation, that is, the percentage of maximum instantaneous spontaneous muscle contraction, which refers to the ratio of the strength generated by specific muscles or muscle groups to their maximum endurance during human exercise, reflecting the degree of muscle participation [26]. When the value is greater than 1, it shows that the muscle is overstressed, in a state of fatigue or even strain, exceeding the maximum tolerance that the human muscle can withstand, and it is easy to cause secondary damage to the user. Therefore, muscle activation must be less than 1. When the muscle is activated, its length will appear nonlinear changes related to muscle tension [27]. Muscle force refers to the ability of the body or a specific part of the body to overcome internal and external resistance during muscle contraction or extension [28].

The human model used in the simulation here is an adult male model with a height of 175 cm and a weight of 70 kg, and the quality attribute of 2.3 kg of the unilateral 2-SPS-RRR parallel mechanism is given to ensure that the simulation is consistent with the actual situation. The right thigh of the human body is simulated for 10s. The static platform of the 2-SPS-RRR parallel mechanism is fixed to the waist of the human body through the joint node, and the moving platform is fixed to the right leg of the human body. The appropriate driving functions are added to the mobile drive P_1, P_2 and the rotational drive θ_1, so that the right leg of the human body can perform flexion and extension, adduction and abduction, internal rotation and external rotation, respectively, taking the gluteus minimus, gluteus medius and piriformis in the main muscle groups near the hip joint of the human body as the research object of dynamic simulation, the muscle length, muscle activation and muscle force change curve of the human gluteus minimus, gluteus medius and piriformis are obtained, as shown in Fig. 11.

It can be seen from Fig. 11 that when the human-robot coupling system is active in the direction of flexion, the muscle length of gluteus minimus is shortened from 114 mm to 107 mm, with a change of 7 mm; the muscle length of the gluteus medius muscle increased from 102 mm to 103.5 mm, with a change of 1.5 mm; the muscle length of the piriformis muscle was shortened from 127.5 mm to 127 mm, with a change of 0.5 mm. It shows that the gluteus minimus is the main muscle to complete the flexion direction, and the gluteus medius and piriformis play a supporting role, at the same time, it shows that the mechanism regulates the muscle length and may optimize its muscle performance. The muscle activation degree of gluteus minimus, gluteus medius and piriformis in the direction of flexion movement changed by 0.0125, 0.015 and 0.02, respectively, and the maximum was 0.0475, 0.0475 and 0.06, respectively, which were much lower than 1, indicating that the hip joint muscle group involved in forward flexion movement was activated to a certain extent, while always maintaining lower than the maximum bearing strength of the muscle, avoiding muscle fatigue or even injury. The force of gluteus minimus increased from 24 N to 32 N, with a change of 8 N. The force of gluteus medius increased from 40 N to 53 N, changed by 13 N; the force of the piriformis increased from 20 N to 34 N, with a change of 14 N. The force of the three muscles reaches the maximum at 10 s, and the change process is gentle and without mutation. It shows that when 2-SPS-RRR spherical parallel mechanism is used for rehabilitation training, the human muscle group can get a certain exercise effect, and the safety in the process of movement is ensured, and the reinjury to the user is avoided.

In addition to the flexion movement, during the extension, adduction, abduction, internal rotation and external rotation movements, the length, activation and force of the

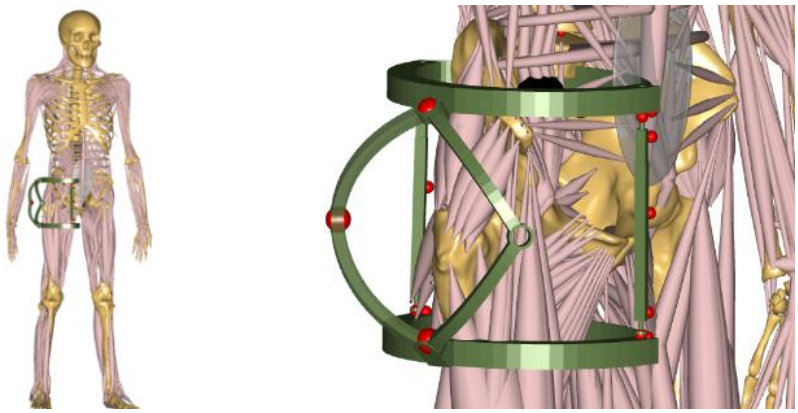

a b

Fig. 10 Human-robot coupling model based on AnyBody: a – complete view model, b – local view model

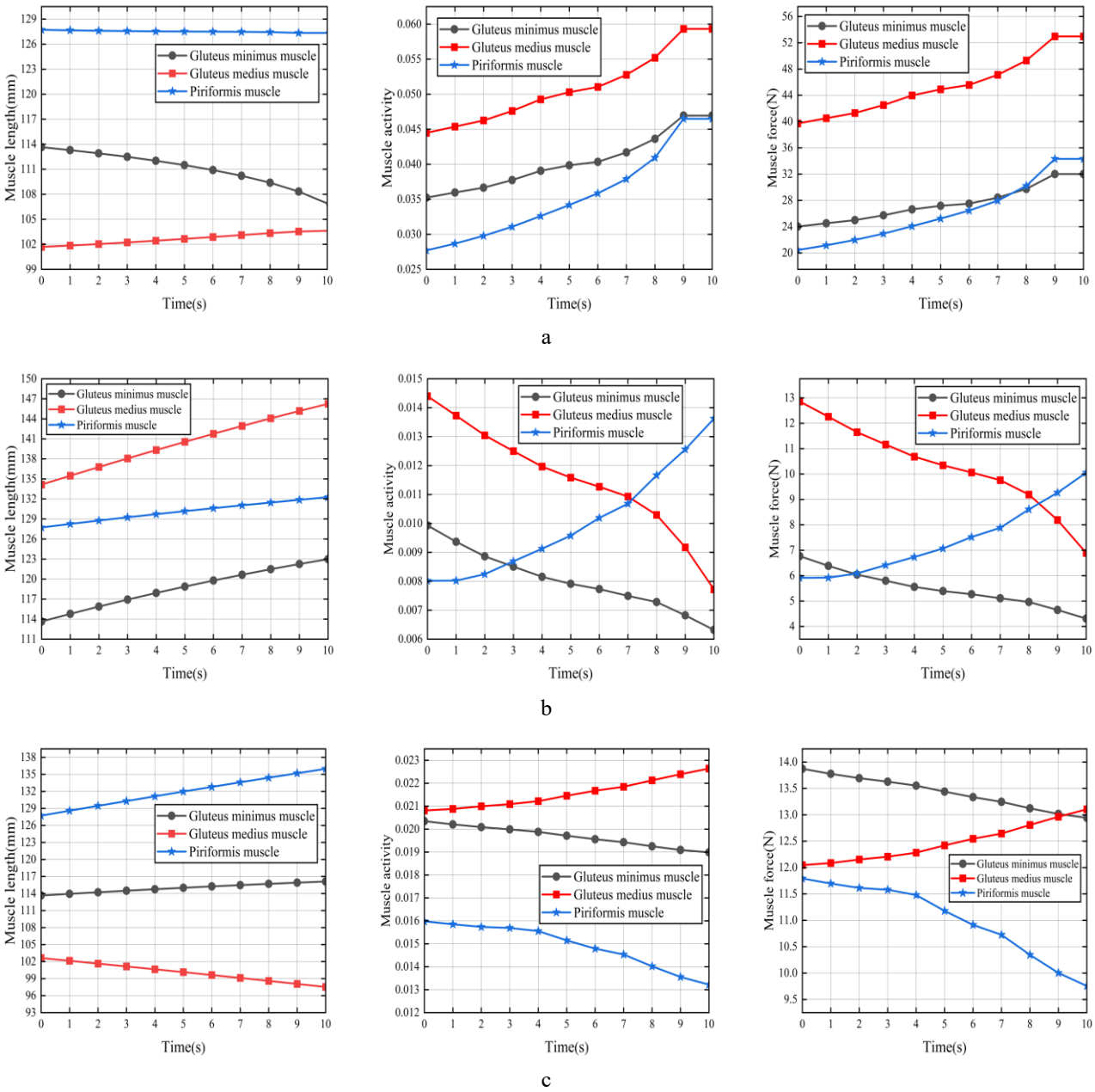

Fig. 11 The curves of the length, activation, and force changes of the gluteus minimus, gluteus medius, and piriformis muscles during flexion, extension, adduction, abduction, internal rotation, and external rotation movements: a – flexion movement, b – adduction movement, c – internal rotation movement

three muscles have a certain degree of change, and the muscle activation degree is far lower than 1 at the same time of change ; at the same time, the force changes of the three muscles are gentle and there is no sudden change, indicating that the muscle group has not only been effectively exercised, but also ensured that the force of the muscle is always within a safe range, and it is not easy to appear fatigue or damage. The risk of muscle strain is reduced, the safety index is high, the secondary damage of the user's rehabilitation process is avoided, and the stability and reliability of the rehabilitation performance of the mechanism are guaranteed.

7. Conclusion

A wearable and adjustable spherical hip exoskeleton parallel mechanism is proposed for the people whose hip joint movement function is damaged due to sudden accidents or natural aging. The mechanism has three rotational degrees of freedom around *X* axis, *Y* axis and *Z* axis, and can realize sagittal plane movements, frontal plane movements and transverse plane movements at the hip joint.

In order to ensure that the motion center of the mechanism coincides with the rotation center of the hip joint after wearing by people of different body types, an adjustable center structure is designed.

By analyzing the workspace and dexterity of the mechanism, it is concluded that the mechanism has a large working range and good performance, which can meet the design requirements. The human-robot coupling simulation based on AnyBody shows that the mechanism is effective for the rehabilitation exercise of human muscle groups, and can meet the rehabilitation needs of patients hip joints.

Acknowledgements

This research was funded by the key research and development project of Shanxi province (Grant Nos. 201903D421051) and the funding project of Shanxi Provincial Basic Research Plan (Grant Nos. 202203021211101).

References

1. **Chen, L. K.** 2022. Urbanization and population aging: Converging trends of demographic transitions in modern world, Archives of Gerontology and Geriatrics 101: 104709. https://doi.org/10.1016/j.archger.2022.104709.
2. **Ferreira, M. L.; de Luca, K.; Haile, L. M.; Steinmetz, J. D.; Culbreth, G. T.; Cross, M.; Kopec, J. A.; Ferreira, P. H.; Blyth, F. M.; Buchbinder, R.; Hartvigsen, J.; Wu, A. M.; Safiri, S.; Woolf, A. D.; Collins, G. S.; Ong, K. L.; Vollset, S. E.; Smith, A. E.; Cruz, J. A.; ... Abdelalim, A.** 2023. Global, regional, and national burden of low back pain, 1990–2020, its attributable risk factors, and projections to 2050: a systematic analysis of the Global Burden of Disease Study 2021, The Lancet Rheumatology 5(6): e316-e329. https://doi.org/10.1016/S2665-9913(23)00098-X.
3. **Miyachi, R.; Sano, A.; Tanaka, N.; Tamai, M.; Miyazaki, J.** 2021. Relationships among lumbar hip motion angle, perceptual awareness, and low back pain in young adults, Journal of Physical Therapy Science 33(12): 880-886. https://doi.org/10.1589/jpts.33.880.
4. **Xu, S.; Tang, K.; Xu, L.; Ding, Y.** 2024. Design, Analysis, and Validation of a Passive Parallel Continuum Ankle Exoskeleton for Support and Walking Assistance, ASME Journal of Mechanisms and Robotics 17(3): 031003. https://doi.org/10.1115/1.4066136.
5. **Yu, S. Y.; Huang, T. H; Yang, X.; Jiao, C.; Yang, J.; Chen, Y.; Yi, J.; Su, H.** 2020. Quasi-Direct Drive Actuation for a Lightweight Hip Exoskeleton With High Backdrivability and High Bandwidth, IEEE/ASME Transactions on Mechatronics 25(4): 1794-1802. https://doi.org/10.1109/TMECH.2020.2995134.
6. **Zhou, T.; Xiong, C.; Zhang, J.; Hu, D.; Chen, W.; Huang, X.** 2021. Reducing the metabolic energy of walking and running using an unpowered hip exoskeleton, Journal of NeuroEngineering and Rehabilitation 18: 95. https://doi.org/10.1186/s12984-021-00893-5.
7. **HONDA.** 2008. Honda's stride management assist device [online] MPRA [accessed 1 May, 2023]. Available from Internet: http://corporate.honda.com/innovation/walk-assist/.
8. **Zheng, E.; Manca, S.; Yan, T.; Parri, A.; Vitiello, N.; Wang, Q.** 2017. Gait Phase Estimation Based on Noncontact Capacitive Sensing and Adaptive Oscillators, IEEE Transactions on Biomedical Engineering 64(10): 2419-2430. https://doi.org/10.1109/TBME.2017.2672720.
9. **Giovacchini, F.; Vannetti, F.; Fantozzi, M.; Cempini, M., Cortese, M., Parri, A.; Yan, T.; Lefeber, D.; Vitiello, N.** 2015. A lightweight active orthosis for hip movement assistance, Robotics and Autonomous Systems 73: 123-134. https://doi.org/10.1016/j.robot.2014.08.015.
10. **Chen, B.; Lanotte, F.; Grazi, L.; Vitiello, N.; Crea, S.** 2019. Classification of Lifting Techniques for Application of A Robotic Hip Exoskeleton, Sensors 19(4): 963. https://doi.org/10.3390/s19040963.
11. **Wang, X. Y.; Chen, C. J.; Ma, Y.; Cao, W. J.; Wu, X. Y.** 2024. Design of a Parallel Hip Exoskeleton and Its System Implementation Based on Human-Machine Integrated Dynamics, Robots 46(3): 339-350 (in Chinese). https://doi.org/10.13973/j.cnki.robot.230149.
12. **Wang, X. Y.; Guo, S.; Qu, B.; Bai, S. P.** 2022. Design and Experimental Verification of a Hip Exoskeleton Based on Human–Machine Dynamics for Walking Assistance, IEEE Transactions on Human-Machine Systems 53(1): 85-97. https://doi.org/10.1109/THMS.2022.3217971.
13. **Xu, J. L.; Liu, F. C.; Niu, Y. Z.** 2023. Design and Analysis of a Novel Weak-coupling Parallel Hip Exoskeleton with Large Angle of Rotation, China Mechanical Engineering 34(21): 2540-2547 (in Chinese). https://doi.org/10.3969/j.issn.1004-132X.2023.21.003.
14. **Shi, D.; Zhang, W.; Zhang, W.; Ju, L.; Ding, X.** 2021. Human-centred adaptive control of lower limb rehabilitation robot based on human–robot interaction dynamic model, Mechanism and Machine Theory 162: 104340. https://doi.org/10.1016/j.mechmachtheory.2021.104340.
15. **Li, J. F.; Li, S.; Zhang, L.; Tao, C.; Ji, R.** 2018. Position solution and kinematic interference analysis of a novel parallel hip-assistive mechanism, Mechanism and Machine Theory 120: 265-287.

https://doi.org/10.1016/j.mechmachtheory.2017.10.002.
16. **Jia, Z. Y.; Li, R. Q.; Liu, J.; Wang, Y.** 2023. Dynamic Modeling and Performance Analysis of a Hip Rehabilitation Robot, Biomimetics 8(8): 585. https://doi.org/10.3390/biomimetics8080585.
17. **Huang, Y.; Li, H.; Gao, Y.; Yang, L.** 2023. Structure design of hip joint parallel rehabilitation exoskeleton, Chinese Journal of Medical Instrumentation 47(6): 612-616. https://doi.org/10.3969/j.issn.1671-7104.2023.06.005.
18. **Cai, Y. B.** 2018. Design and Study on a Parallel Hip Joint Rehabilitation Robot with Adjustable Center of Rotation, Qinhuangdao Yanshan University (in Chinese).
19. **Chen, W. B.; Zhang, Y. L.; Fu, H.; Fan, X.; Xiong, C. H.; Liang, J. J.** 2022. Optimization design of prosthetic shoulder joint based on three-RRR asymmetric spherical parallel mechanism, Scientia Sinica Technologica 52(9): 1434-1446. https://doi.org/10.1360/SST-2021-0425.
20. **Cao, L.** 2019. Performance analysis and optimization design of parallel ball and socket joint rehabilitation mechanism, Taiyuan North University of China (in Chinese).
21. **Ma, S.** 2017. Research on active and passive driven lower limbs powered exoskeleton robot (Master's thesis), Harbin Institute of Technology: 18-20 (in Chinese).
22. **Shang, L. J.; Hu, Z. A.** 2014. Muscle force analysis of hiprehabilitation training based on AnyBody, Journal of Dalian Jiaotong University 35(1): 50-52 (in Chinese).
23. **Huang, Z.; Zhao, Y. S.; Zhao, T. S.** 2014. Advanced Spatial Mechanism (Second Edition), Beijing Higher Education Press: 111-152 (in Chinese).
24. **Kong, X.; Gosselin, C.** 2007. Virtual-chain approach for the type synthesis of parallel mechanisms. In: Type Synthesis of Parallel Mechanisms (33: 63-83). Springer, Berlin, Heidelberg. https://doi.org/10.1007/978-3-540-71990-8_5.
25. **Rosyid, A.; El-Khasawneh, B.; Alazzam, A.** 2020. Performance measures of parallel kinematics manipulators, Mechanical Sciences 11(1): 49-73. https://doi.org/10.5194/ms-11-49-2020.
26. **Grazi, L.; Trigili, E.; Proface, G.; Giovacchini, F.; Crea, S.; Vitiello, N.** 2020. Design and Experimental Evaluation of a Semi-Passive Upper-Limb Exoskeleton for Workers With Motorized Tuning of Assistance, IEEE Transactions on Neural Systems and Rehabilitation Engineering 28(10): 2276-2285. https://doi.org/10.1109/TNSRE.2020.3014408.
27. **Weinstock-Zlotnick, G.; Mehta, S. P.** 2019. A systematic review of the benefits of occupation-based intervention for patients with upper extremity musculoskeletal disorders, Journal of Hand Therapy 32(2): 141-152. https://doi.org/10.1016/j.jht.2018.04.001.
28. **Del, Ferraro. S.; Falcone, T.; Ranavolo, A.; Molinaro, V.** 2020. he Effects of Upper-Body Exoskeletons on Human Metabolic Cost and Thermal Response during Work Tasks—A Systematic Review, International Journal of Environmental Research and Public Health 17(20): 7374. https://doi.org/10.3390/ijerph17207374.

Y. H. Zhao, Y. F. Zhang, Y. Gao, R. Q. Li

STUDY ON THE REHABILITATION PERFORMANCE OF 2-SPS-RRR ADJUSTABLE HIP EXOSKELETON

S u m m a r y

Based on computer-aided ergonomics the paper proposes a hip joint rehabilitation exoskeleton utilizing a adjustable spherical parallel mechanism, specifically designed for rehabilitation training of individuals with impaired hip joint movement function. Initially, the screw theory is employed to determine the degrees of freedom of the parallel mechanism, revealing that it possesses three rotational degrees of freedom, enabling sagittal plane movements, frontal plane movements and transverse plane movements at the hip joint. The closed vector method is utilized to derive the inverse position solution, and the velocity Jacobian matrix is solved. Leveraging the inverse position solution and the constraint relationships between mechanisms, the reachable workspace of the mechanism is obtained using MATLAB software programming. Utilizing screw theory and velocity Jacobian matrix, the dexterity of the mechanism is analyzed. Ultimately, a human-robot integrated system is established in AnyBody software to verify its capability to achieve certain rehabilitation effects on human muscle groups. Research demonstrated that the hip joint parallel mechanism exhibits good stability and can effectively assist individuals with hip joint dysfunction in rehabilitation training.

Keywords: hip exoskeleton, spherical parallel mechanism, kinematics, rehabilitation performance.

Received June 7, 2026
Accepted April 24, 2026

Appendix A

$$a_1 = \left(rc_\theta c_\phi - m\left(s_\psi s_\theta c_\phi - c_\psi s_\phi\right) - l\left(c_\psi s_\theta c_\phi + s_\psi s_\phi\right) - R\right)\left(-ms_\theta c_\phi c_\psi - mc_\phi s_\psi + ls_\theta c_\phi s_\psi - lc_\psi s_\phi\right) +$$
$$+\left(rc_\theta s_\phi - m\left(s_\psi s_\theta s_\phi + c_\psi c_\phi\right) - l\left(c_\psi s_\theta s_\phi - s_\psi c_\phi\right) + m\right)\left(-ms_\theta s_\phi c_\psi + mc_\phi s_\psi + ls_\theta s_\phi s_\psi + lc_\psi c_\phi\right) +$$
$$+\left(-rs_\theta - ms_\psi c_\theta - lc_\psi c_\theta - l\right)\left(-mc_\psi c_\theta + ls_\psi c_\theta\right),$$

$$b_1 = \left(rc_\theta c_\phi - m\left(s_\psi s_\theta c_\phi - c_\psi s_\phi\right) - l\left(c_\psi s_\theta c_\phi + s_\psi s_\phi\right) - R\right)\left(-rc_\phi s_\theta - ms_\psi c_\phi c_\theta - lc_\psi c_\phi c_\theta\right) +$$
$$+\left(rc_\theta s_\phi - m\left(s_\psi s_\theta s_\phi + c_\psi c_\phi\right) - l\left(c_\psi s_\theta s_\phi - s_\psi c_\phi\right) + m\right)\left(-rs_\phi s_\theta - ms_\psi s_\phi c_\theta - lc_\psi s_\phi c_\theta\right) +$$
$$+\left(-rs_\theta - ms_\psi c_\theta - lc_\psi c_\theta - l\right)\left(-rc_\theta + ms_\psi s_\theta + lc_\psi s_\theta\right),$$

$$c_1 = \left(rc_\theta c_\phi - m\left(s_\psi s_\theta c_\phi - c_\psi s_\phi\right) - l\left(c_\psi s_\theta c_\phi + s_\psi s_\phi\right) - R\right)\left(-rc_\theta s_\phi + ms_\psi s_\theta s_\phi + mc_\psi c_\phi + lc_\psi s_\theta s_\phi - ls_\psi c_\phi\right) +$$
$$+\left(rc_\theta s_\phi - m\left(s_\psi s_\theta s_\phi + c_\psi c_\phi\right) - l\left(c_\psi s_\theta s_\phi - s_\psi c_\phi\right) + m\right)\left(rc_\theta c_\phi - ms_\psi s_\theta c_\phi + mc_\psi s_\phi - lc_\psi s_\theta c_\phi - ls_\psi s_\phi\right),$$

$$d_1 = \sqrt{\begin{array}{l}\left(rc_\theta c_\phi - m\left(s_\psi s_\theta c_\phi - c_\psi s_\phi\right) - l\left(c_\psi s_\theta c_\phi + s_\psi s_\phi\right) - R\right)^2 + \left(r\,c_\theta s_\phi - m\left(s_\psi s_\theta s_\phi + c_\psi c_\phi\right) - \right. \\ \left. -l\left(c_\psi s_\theta s_\phi - s_\psi c_\phi\right) + m\right)^2 + \left(-rs_\theta - ms_\psi c_\theta - lc_\psi c_\theta - l\right)^2,\end{array}}$$

$$a_2 = \left(-rc_\theta c_\phi - m\left(s_\psi s_\theta c_\phi - c_\psi s_\phi\right) - l\left(c_\psi s_\theta c_\phi + s_\psi s_\phi\right) + R\right)\left(-ms_\theta c_\phi c_\psi - mc_\phi s_\psi + ls_\theta c_\phi s_\psi - lc_\psi s_\phi\right) +$$
$$+\left(rc_\theta s_\phi - m\left(s_\psi s_\theta s_\phi + c_\psi c_\phi\right) - l\left(c_\psi s_\theta s_\phi - s_\psi c_\phi\right) + m\right)\left(-ms_\theta s_\phi c_\psi + mc_\phi s_\psi + ls_\theta s_\phi s_\psi + lc_\psi c_\phi\right) +$$
$$+\left(-rs_\theta - ms_\psi c_\theta - lc_\psi c_\theta - l\right)\left(-mc_\psi c_\theta + ls_\psi c_\theta\right),$$

$$b_2 = \left(-rc_\theta c_\phi - m\left(s_\psi s_\theta c_\phi - c_\psi s_\phi\right) - l\left(c_\psi s_\theta c_\phi + s_\psi s_\phi\right) + R\right)\left(rc_\phi s_\theta - ms_\psi c_\phi c_\theta - lc_\psi c_\phi c_\theta\right) + \left(rc_\theta s_\phi - m\left(s_\psi s_\theta s_\phi + c_\psi c_\phi\right)\right.$$
$$\left.-l\left(c_\psi s_\theta s_\phi - s_\psi c_\phi\right) + m\right)\left(-rs_\phi s_\theta - ms_\psi s_\phi c_\theta - lc_\psi s_\phi c_\theta\right) + \left(-rs_\theta - ms_\psi c_\theta - lc_\psi c_\theta - l\right)\left(-rc_\theta + ms_\psi s_\theta + lc_\psi s_\theta\right),$$

$$c_2 = \left(-rc_\theta c_\phi - m\left(s_\psi s_\theta c_\phi - c_\psi s_\phi\right) - l\left(c_\psi s_\theta c_\phi + s_\psi s_\phi\right) + R\right)\left(rc_\theta s_\phi + ms_\psi s_\theta s_\phi + mc_\psi c_\phi + lc_\psi s_\theta s_\phi - ls_\psi c_\phi\right) +$$
$$+\left(rc_\theta s_\phi - m\left(s_\psi s_\theta s_\phi + c_\psi c_\phi\right) - l\left(c_\psi s_\theta s_\phi - s_\psi c_\phi\right) + m\right)\left(rc_\theta c_\phi - ms_\psi s_\theta c_\phi + mc_\psi s_\phi - lc_\psi s_\theta c_\phi - ls_\psi s_\phi\right),$$

$$d_2 = \sqrt{\begin{array}{l}\left(-rc_\theta c_\phi - m\left(s_\psi s_\theta c_\phi - c_\psi s_\phi\right) - l\left(c_\psi s_\theta c_\phi + s_\psi s_\phi\right) + R\right)^2 + \left(r\,c_\theta s_\phi - m\left(s_\psi s_\theta s_\phi + c_\psi c_\phi\right) - \right. \\ \left. -l\left(c_\psi s_\theta s_\phi - s_\psi c_\phi\right) + m\right)^2 + \left(-rs_\theta - ms_\psi c_\theta - lc_\psi c_\theta - l\right)^2,\end{array}}$$

$$a_3 = \left(l\tan(50) + r\right)\left(\left(s_\phi s_\psi + c_\phi s_\theta c_\psi\right)\left(2l - \left(l\tan(50) + r\right)c_\theta s_\psi\right) - \left(-l\tan(50) - r\right)c_\theta c_\psi\left(c_\phi s_\theta s_\psi - s_\phi c_\psi\right)\right),$$

$$b_3 = \left(l\tan(50) + r\right)\left(\left(-l\tan(50) - r\right)s_\psi s_\theta\left(c_\phi s_\psi s_\theta - s_\phi c_\psi\right) + c_\phi s_\psi c_\theta\left(2l - \left(l\tan(50) + r\right)s_\psi c_\theta\right)\right),$$

$$c_3 = \left(l\tan(50) + r\right)\left(-s_\psi s_\theta s_\phi - c_\psi c_\phi\right)\left(2l - \left(l\tan(50) + r\right)s_\psi c_\theta\right),$$

$$d_3 = \left(2l - \left(l\tan(50) + r\right)c_\theta s_\psi\right)^2\left(\frac{\left(l\tan(50) + r\right)^2\left(c_\phi s_\theta s_\psi - s_\phi c_\psi\right)^2}{\left(2l - \left(l\tan(50) + r\right)c_\theta s_\psi\right)^2} + 1\right).$$